




Competing correlated insulators in multiorbital systems coupled to phonons

Alberto Scazzola ¹, Adriano Amaricci ², and Massimo Capone ^{1,2}

¹*Scuola Internazionale Superiore di Studi Avanzati (SISSA), Via Bonomea 265, I-34136 Trieste, Italy*

²*CNR-IOM Democritos, Via Bonomea 265, I-34136 Trieste, Italy*



(Received 1 December 2021; revised 25 January 2023; accepted 27 January 2023; published 21 February 2023)

We study the interplay between electron-electron interaction and a Jahn-Teller phonon coupling in a two-orbital Hubbard model. We demonstrate that the e-ph interaction coexists with the Mott localization driven by the Hubbard repulsion U , but it competes with the Hund's coupling J . This interplay leads to two spectacularly different Mott insulators, a standard high-spin Mott insulator with frozen phonons which is stable when the Hund's coupling prevails, and a low-spin Mott-bipolaronic insulator favored by phonons, where the characteristic features of Mott insulators and bipolarons coexist. The two phases are separated by a sharp boundary along which an intriguing intermediate solution emerges as a kind of compromise between the two solutions.

DOI: [10.1103/PhysRevB.107.085131](https://doi.org/10.1103/PhysRevB.107.085131)

I. INTRODUCTION

Electron-phonon (e-ph) coupling and electron-electron (e-e) repulsion are the key interactions determining the properties of electrons in solids. Their relative importance can vary significantly across different classes of materials, often leading to the neglect of one or the other in theoretical treatment. On the other hand, it is nowadays clear that the interplay between e-e and e-ph interaction plays an important role in a wide class of materials, from colossal magnetoresistance manganites [1] to different families of high-temperature superconductors [2–12].

A wide majority of studies of the interplay between the two interactions is based on a single-band Hubbard-Holstein (HH) model featuring an on-site Hubbard repulsion and a coupling between the local electron density and phonons [13–41]. The simplicity of the HH model may lead one to identify it as the paradigm to study the two interactions, but this expectation is somewhat misleading, i.e., that the properties of this model are not as generic as expected. Indeed, in the HH model the phonons give rise to a frequency-dependent local attraction which has the same form of the Hubbard repulsion. Thus, the two interactions directly compete and the physics is essentially controlled by the comparison of the coupling strengths. The only nontrivial interplay arises because the U term is instantaneous and the phonon term is retarded [17]. A richer outcome can be realized in single-band systems considering nonlocal e-ph couplings which compete less directly with the repulsion [42–47].

On the other hand, a single-band model is not adequate for a large number of correlated materials. Multiorbital models with e-e interaction have been widely investigated recently, emphasizing the nontrivial role of the Hund's coupling in the physics of strong correlations and its relevance for different materials [48,49].

In this work we extend the study of the interplay between e-e correlations and e-ph coupling to multiorbital systems

by solving a two-orbital model including e-e interaction, parametrized by the Hubbard U and the Hund's coupling J , and a Jahn-Teller (JT) e-ph mode. Using dynamical mean-field theory (DMFT) [50] we focus on the different strongly correlated phases originating from the interplay of these two interactions.

This study is not designed to model any specific material, but rather to identify general phenomena characterizing e-ph interaction in correlated materials, similarly to studies of the role of the Hund's coupling in models [48] which have been instrumental to understand their role in iron-based superconductors [51] and ruthenates [52]. In the same spirit, the present results can be of direct relevance for a wide class of materials where JT phonons and e-e interactions are both relevant, including, among others, fullerides [9,16,53,54], manganites [1,55], chromates [56,57], and magic-angle twisted bilayer graphene [58].

Our results show that the JT phonon mode *cooperates* with the Hubbard interaction, but it competes with the Hund's exchange J . The prevalence of either the Hund coupling or JT e-ph coupling favors different strongly correlated Mott-like phases with remarkably distinct properties, i.e., a high-spin Mott insulator and a low-spin Mott-bipolaronic state where phonon fingerprints and Mott physics coexist. Finally, we identify a hybrid Mott insulator resulting from a perfect balance between the effects of the e-ph and the Hund's couplings.

II. MODEL AND SOLUTION

We consider a two-orbital Hubbard model with two degenerate bands described by a semicircular density of states with half-bandwidth D ,

$$\mathcal{D}(\epsilon) = \frac{2}{\pi D^2} \sqrt{D^2 - \epsilon^2}, \quad |\epsilon| < D, \quad (1)$$

which is realized on a Bethe lattice.

The e-e interaction is

$$H_{e-e} = U \sum_{i,a} n_{ia\uparrow} n_{ia\downarrow} + (U - 3J) \sum_{i,a<b,\sigma} n_{ia\sigma} n_{ib\sigma} + (U - 2J) \sum_{i,a\neq b} n_{ia\uparrow} n_{ib\downarrow}, \quad (2)$$

where i , a and b , σ are respectively site, orbital, and spin indices. This popular form of the interaction can be seen as a Kanamori model without spin-flip and pair-hopping terms [59,60]. A dispersionless mode of frequency ω_0 is coupled with the difference in the occupation between the two orbitals, i.e., the orbital polarization:

$$H_{e-ph} = g \sum_{i\sigma} (n_{i1\sigma} - n_{i2\sigma})(a_i^\dagger + a_i) + \omega_0 \sum_i a_i^\dagger a_i. \quad (3)$$

This term corresponds to one of the two JT modes of a two-orbital e_g manifold (usually referred to as Q_3 and corresponding to an orthorhombic distortion which makes the z axis inequivalent to the xy plane). We did not include the other JT mode to keep the number of parameters relatively small, while the Holstein coupling is expected to reproduce the single-band results [61,62].

We set the density to half filling $n = 2$ for which the interactions can have qualitative effects, e.g., the e-e interaction can lead to a Mott insulator. We define $\lambda = 2g^2/\omega_0$ as the strength of the phonon-induced attraction.

We solve the model using DMFT, which maps the lattice problem onto a quantum impurity model subject to a self-consistency condition which contains the information on the lattice model. In our model, since the e-ph coupling and the bare phononic Hamiltonian are local, the impurity model also includes a phononic term on the impurity site, while the bath remains purely fermionic [63]. DMFT allows for a nonperturbative solution treating the two interaction terms on the same footing without assuming any hierarchy between the different energy scales of the problem. We solve the impurity model at $T = 0$ using exact diagonalization [64–66] after a truncation of the impurity model to a small number of levels, that we typically take as $N_l = 8$, and to a limited number of phononic levels, that we typically fix to $N_{\text{max}}^{\text{ph}} = 25$. The convergence with respect to these parameters has been tested as discussed in the Supplemental Material [60]. We do not allow for any broken-symmetry solution, including charge-, spin-, and orbital-ordering and superconductivity. This choice allows us to identify the intrinsic correlation effects resulting from the various interactions and their interplay.

We characterize the metal-insulator transitions using the quasiparticle weight Z which measures the degree of metallicity of the system, the intraorbital double occupation $\langle n_{im\uparrow} n_{im\downarrow} \rangle$ with $m = 1, 2$ and the local magnetic moment measured by $\langle S_z^2 \rangle = \langle (\sum_m S_{zim})^2 \rangle$. All quantities do not depend on the site index i that we drop in the following. We also monitor the phonons via the number of excited phonons $N_{\text{ph}} = \langle a^\dagger a \rangle$ and the phonon distribution function $P(X)$ which measures the quantum amplitude that the phonon displacement operator assumes a value X .

Our model depends on four independent parameters U/D , J/D , λ/D , and ω_0/D . In the following we will keep the ratios U/J and λ/J constant when considering $J > 0$, while we

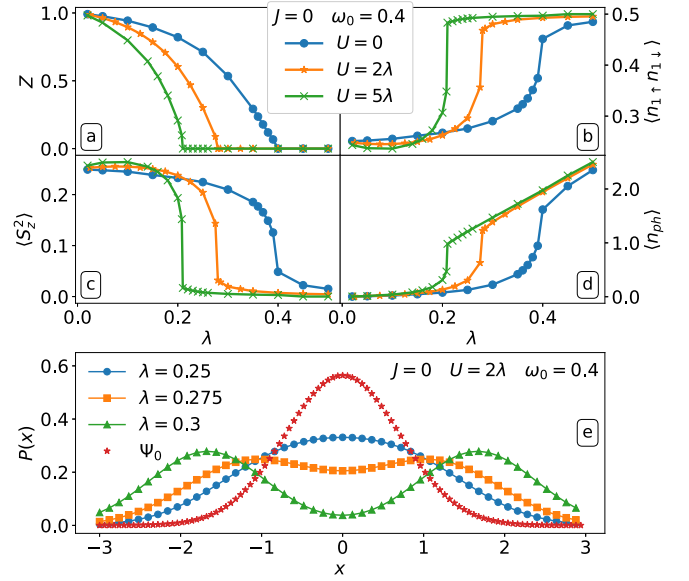


FIG. 1. Approach to the bipolaronic-Mott insulator for $J = 0$. (a)–(d) Evolution of Z , $\langle n_{im\uparrow} n_{im\downarrow} \rangle$, $\langle S_z^2 \rangle$, and $\langle n_{\text{ph}} \rangle$ as a function of λ for three different values of U/λ and $\omega_0/D = 0.4$. (e) Evolution of the phonon distribution function $P(X)$ across the metal-insulator transition for $U/\lambda = 2$ compared with that of an uncoupled phonon Ψ_0 .

vary the e-e interaction strength U/D . This choice mimics the effect of pressure and chemical substitution that change the hopping while leaving the local interactions less affected. We take the ratio ω_0/D as an independent variable in order to measure the effect of the degree of adiabaticity (retardation) of the e-ph coupling.

III. RESULTS

We start our discussion from the limit $J = 0$. In Fig. 1 we report various quantities as a function of λ and three values of U/λ . For $U = 0$ we have pure e-ph interaction. Increasing λ leads to a reduction of the quasiparticle weight Z (enhancement of the effective mass), Fig. 1(a), that eventually vanishes for $\lambda \simeq 0.4$ signaling a metal-insulator transition. The intraorbital double occupancy, Fig. 1(b), evolves toward 0.5 while the squared magnetic moment, Fig. 1(c), falls toward zero. We conclude that we reached an insulating state where every site has two electrons on one of the two orbitals, while the other is empty. Half of the sites have two electrons on orbital 1, the other half on orbital 2. The number of phonons, Fig. 1(d), in the ground state increases sharply as the insulating state is approached. Importantly, the phonon distribution function $P(X)$, Supplemental Material [60] Fig. 2(e), is centered around $X = 0$ in the whole metallic region, but it turns into a bimodal with maxima at $\pm X_0 \neq 0$ at the transition, testifying that the insulator is the two-orbital realization of a bipolaronic state [67,68] where every lattice site has a finite distortion, half with one sign and half with the other. The sites where orbital 1 (2) is doubly occupied have a negative (positive) distortion. The picture does not depend qualitatively on ω_0/D , as we show in the Supplemental Material [60].

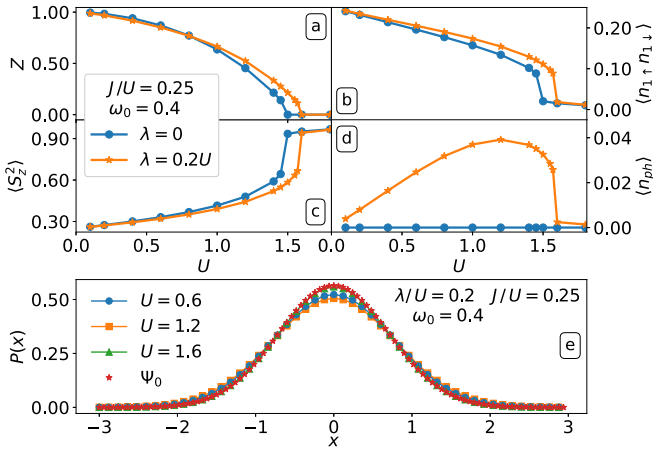


FIG. 2. Approach to the high-spin Mott insulator for zero or small λ . (a)–(d) Evolution of Z , $\langle n_{m\uparrow}n_{m\downarrow} \rangle$, $\langle S_z^2 \rangle$, and $\langle n_{ph} \rangle$ as a function of U/D for two distinct values of λ/U and $\omega_0/D = 0.4$. (e) Evolution of the phonon distribution function $P(X)$ across the metal-insulator transition for $\lambda/U = 0.2$ compared with that of an uncoupled phonon Ψ_0 .

We now switch on the U repulsion, while keeping $J = 0$. Since the ratio U/λ is kept constant, U increases when we increase λ . Remarkably, even if we consider a sizable U larger than λ [$U/\lambda = 2$ and 5 in Figs. 1(a)–1(e)], the picture obtained for $\lambda = 0$ is not destroyed. Indeed all the observables follow the same qualitative behavior of $U = 0$. Even more surprisingly the Hubbard repulsion *favours* the bipolaronic transition, which takes place for smaller λ as U/λ increases. This is in sharp contrast with the results for the Hubbard-Holstein model, for which a large U completely quenches phononic effects [17]. This unexpected result can be easily understood noticing that for $J = 0$ the interaction is $U/2 \sum_i n_i^2$ (with $n_i = \sum_{a\sigma} n_{ia\sigma}$) which simply selects configurations with doubly occupied sites, i.e., configurations where the local occupation equals the average, without any preference for the internal arrangement between the orbitals. If we denote by $|n_1, n_2\rangle$ configurations with n_a electrons in the orbital $a = 1, 2$ we have that $|0, 2\rangle$ and $|2, 0\rangle$, which are favored by the phonons and characterize the bipolaronic state, are also compatible with the effect of U . This in turn helps the e-ph coupling to filter out configurations with different local occupation. Thus, Mott localization and bipolaron formation work in synergy to stabilize a *low-spin Mott-bipolaronic* insulator. Such a state cannot be realized in a single-band model where Mott and bipolaronic insulators are mutually exclusive.

The inclusion of the Hund's coupling changes the picture by favoring high-spin configurations and disfavoring double occupation of the same orbital. In Fig. 2 we show the same quantities as in 1 for fixed ratio $J/U = 0.25$, comparing the results for $\lambda = 0$ with those for $\lambda/U = 0.2$. Without e-ph coupling we recover a two-component Hubbard model. In this case, increasing U induces a Mott transition signaled by a vanishing Z , Fig. 2(a). The presence of J makes the Mott insulator high spin. For density-density interaction, the Mott insulator mainly features configurations with $S = 1$ and $S_z = \pm 1$, completely different from those characterizing the bipolaronic insulator discussed above. Accordingly, when Z

vanishes, the intraorbital double occupation tends to zero, Fig. 2(b), while the magnetic moment increases toward 1, Fig. 2(c).

The inclusion of a moderate e-ph coupling ($\lambda/U = 0.2$) does not alter the picture besides a small increase of the critical interaction strength for the Mott transition. The number of excited phonons, Fig. 2(d), is very small and eventually drops to zero approaching the Mott insulator despite the increasing e-ph coupling. The phonon distribution, Fig. 2(e), remains centered around $X = 0$ and is barely distinguishable from that of uncoupled phonons. In other words the presence of J completely quenches the phonon degrees of freedom at least for these parameters.

We have shown that the competition between λ and J can lead to two completely different strongly correlated phases for large U . In the absence of J we find a low-spin Mott-bipolaronic state, while the prevalence of J over λ leads to a high-spin Mott state without phononic signatures. This confirms the expectation that a JT phonon mode only competes with the Hund's coupling [9,11,12], while its effect can coexist with Mott localization. We can understand and rationalize this result by integrating out the JT mode. This leads to a retarded (frequency-dependent) e-e interaction

$$U^{e-ph}(\omega) = \frac{\omega_0 g^2 (n_1 - n_2)^2}{\omega^2 - \omega_0^2}. \quad (4)$$

In the adiabatic limit $\omega_0 \gg D$ this becomes a static effective interaction

$$U^{\text{eff}} = -\frac{\lambda}{2} (n_1 - n_2)^2 = -\lambda \sum_{i,a} n_{ia\uparrow} n_{ia\downarrow} + \lambda \sum_{i,a<b,\sigma} n_{ia\sigma} n_{ib\sigma} + \lambda \sum_{i,a\neq b} n_{ia\uparrow} n_{ib\downarrow}. \quad (5)$$

The intraorbital repulsion is thus reduced from U to $U - \lambda$, while the interorbital interactions are enhanced to $U - 2J + \lambda$ (opposite spins) and $U - 3J + \lambda$ (parallel spins). Interestingly, this opens the opportunity for an interorbital repulsion larger than the intraorbital one, a situation which is never found in a purely electronic model. We can expect that the high-spin Mott insulator (bipolaronic Mott) will be realized when the effective intraorbital (interorbital) term prevails on the other. The boundary between the two phases can be estimated as $U - \lambda \simeq U - 3J + \lambda$ or $\lambda \simeq \frac{3}{2}J$.

In Figs. 3(a) and 3(b) we show DMFT results for the region around $\lambda/J = 3/2$ with $J/U = 0.2$ and $\omega_0/D = 0.4$. We see that the system evolves toward the high-spin Mott insulator (zero double occupancy, high spin) for $\lambda/J < 3/2$, while it converges toward the Mott-bipolaronic one (large double occupancy, low spin) for $\lambda/J > 3/2$, in agreement with the above estimate. Precisely at $\lambda/J = 3/2$ we find a superposition between the two above solutions where the observables tend to the average of the limiting insulators. For instance, the double occupancy converges toward $1/4$ while the local spin reaches $1/2$. We checked that this *hybrid* Mott state features both the local configurations of the bipolaronic insulator ($|2, 0\rangle$ and $|0, 2\rangle$) and that of the Mott insulator ($|1, 1\rangle$) with equal weights. The nature of the hybrid Mott insulator is further clarified by the behavior of $P(X)$, Fig. 3(c). Increasing U and λ the phonons develop a *trimodal*

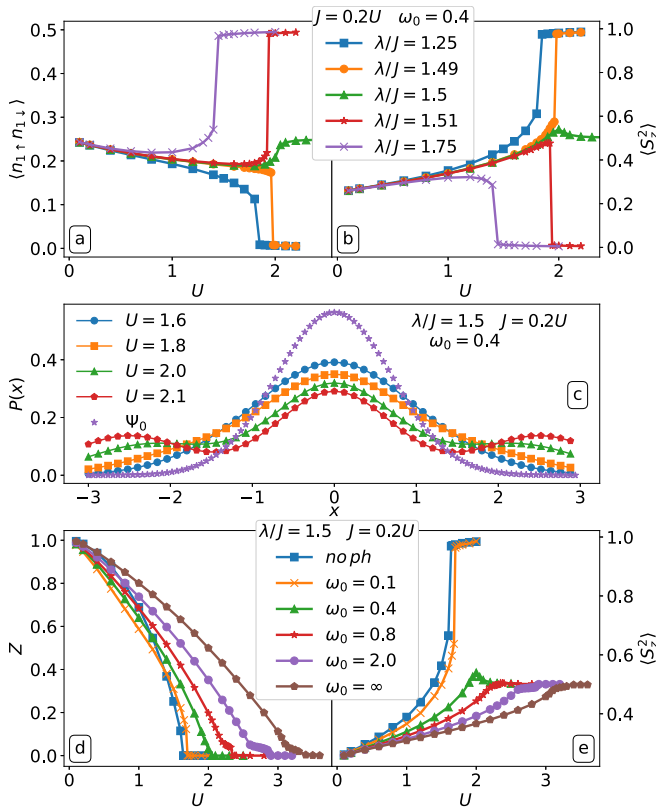


FIG. 3. (a)–(b) Evolution of the intraorbital double occupations (left) and local spin (right) as a function of U/D for different values of λ/J and fixed $J/U = 0.2$. (c) Phonon distribution function $P(X)$ for $\lambda/J = 3/2$ for different U/D . (d)–(e) Evolution of Z and $\langle S_z^2 \rangle$ as a function of U for different values of ω_0/D with $\lambda/J = 3/2$.

distribution with maxima at $X = 0$ and at $X = \pm X_0$, i.e., a superposition of the distributions of the two paradigmatic insulators.

We notice that, unlike similar systems described by a multi-orbital Hubbard model showing a Hund’s metal solution at the boundary between two insulators [69,70], the hybrid solution bridging between two paradigmatic insulators is not metallic. The reason is that all the local configurations characterizing the hybrid state have the same occupation and they cannot be connected by hopping processes. We finally discuss the role of the phonon frequency ω_0 , Figs. 3(d) and 3(e). Interestingly the simple analytical estimate for the transition between the insulators obtained in the adiabatic limit agrees with DMFT data also down to $\omega_0/D < 1$, suggesting that retardation effects come into play only close to the limit $\omega_0 \rightarrow 0$. The hybrid insulator is indeed realized when $\omega_0/D > 0.2$. For smaller ω_0 we recover the behavior of the purely electronic model. Finally, the critical U for the hybrid Mott state decreases by reducing ω_0/D .

Our main conclusions can be summarized in the schematic phase diagram of Fig. 4 in the J - λ plane (with U proportional to J) where a metallic phase is stable when both interactions are small (we recall that we do not consider broken-symmetry solutions). The strong-coupling solution largely depends on the ratio λ/J between the e-ph and the Hund’s couplings. For small J we find a bipolaronic-Mott insulator (yellow re-

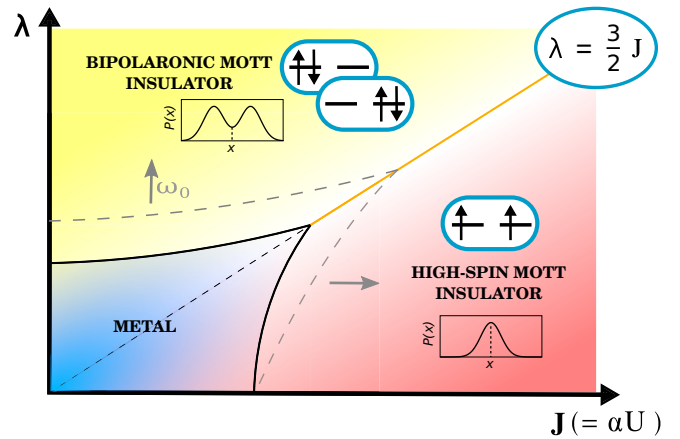


FIG. 4. Schematic phase diagram of our model in the J - λ space. The yellow region is the Mott-bipolaronic state, while the red region is the high-spin Mott insulator. The blue area is the metallic solution. Increasing ω_0 the metallic region extends as shown by the arrows and the gray dashed lines.

gion) where the Mott localization and the tendency to form bipolarons coexist and cooperate. For small λ we have a high-spin Mott insulator (red region) where the phonon fingerprints are washed out by the Hund’s coupling. Setting $\lambda/J = 3/2$ we reach a hybrid Mott insulator which shows features of both the above insulators as shown by a peculiar trimodal phonon distribution. Increasing the phonon frequency enlarges the metallic region.

IV. CONCLUSIONS AND PERSPECTIVES

Our results highlight that the interplay between strong electronic correlations and phonons can be subtle and multifaceted, in contrast with the HH model where the two effects are essentially exclusive. In particular we have regimes where the Mott transition is favored by phonons and phononic fingerprints are clear in the strongly correlated metal and in the Mott insulators, but also regimes where the effect of phonons is completely quenched. The intermediate regime where we have a superposition between the two insulators is particularly intriguing even if it is found only for a specific line of the phase diagram.

This picture has been drawn using DMFT, where the self-energy is local. However, we do not expect nonlocal effects to introduce important changes in our phase diagram due to the local character of our strong-coupling solutions. In Ref. [71] it has been indeed shown, for a Bernevig-Hughes-Zhang-Hubbard model, that nonlocal correlation effects are important only in the weak-coupling region, while single-site DMFT is very close to a cluster-DMFT solution for intermediate and large interactions where the phase transitions of the model take place. Accordingly, we expect that nonlocal correlations can be relevant in the region of small U , λ , and J where they can affect the metallic region and lead to lattice-dependent instabilities.

We also expect that, similarly to the Mott transition and the bipolaronic transition, our $T = 0$ results will extend to a range of temperature corresponding to a small fraction of the

bandwidth, i.e., a hundred of kelvins if we consider the typical scales of oxides, making them relevant for real materials.

As we mentioned in the introduction, the present work is not meant to describe any specific material, but it is rather used as a basic simple model in order to identify key physical phenomena to guide more realistic studies of specific materials. Still, we can mention a few systems where the ideas we discussed are expected to be relevant. The key role of the competition between the Hund's coupling and JT phonons has already been discussed in the alkali-doped fullerenes [9,16,53,54], but the role of a finite phonon frequency and its effect on the normal-state properties have not been discussed in equal detail. *Ab initio* evaluations of the various electronic and phononic parameters [11,12] have shown that, at low energy, the electron-phonon contribution λ is larger in strength with respect to the Hund's coupling, while they are both smaller than the Hubbard U . For instance, for K_3C_{60} , $U = 0.82$ eV, while $J = 31$ meV and $\lambda = 50$ meV. This would put the material in the metallic region close to the $\lambda = 3/2J$ line (notice however that fullerenes are described by a three-orbital model which makes a quantitative comparison questionable).

The physics that we discussed can be relevant also for alkaline-earth chromates ACrO_3 ($A = \text{Ca}, \text{Sr}, \text{Ba}$) where different correlated phases have been observed. BaCrO_3 is a Mott insulator in which Hund's physics and Jahn-Teller distortions play a role [56], while the other two compounds appear to be at the border between insulating and metallic states. In particular, it has been recently proposed based on DFT+ U calculations [57] that for realistic values of $U \simeq 2$ eV SrCrO_3 is a correlated metal which turns insulating in the presence of a strain which can be related to the JT splitting. In particular, increasing U favors the onset of the JT distortion, in agreement with the behavior we find in the Mott-bipolaronic state. This confirms a scenario in which the JT distortion cooperates with the Hubbard U stabilizing an insulator, as well as the relevance

of the Hund's coupling and the proximity between different states in which the interplay between the various interactions has different outcomes.

Finally, it has been recently proposed that a valley Jahn-Teller effect is active in magic-angle twisted bilayer graphene (MATBG) [58] and it can coexist with Hubbard repulsion to drive a Mott-JT insulator which bears similarities with our Mott-bipolaronic state. In this case, a direct mapping onto our model is not available because of the inherent difficulties to build an effective tight-binding model. Yet, in Ref. [58] it has been estimated that the Coulomb pseudopotential, which can be connected with the Hubbard U , is $\mu^* \simeq 27$ meV, while, for reasonable parameters and different fillings, a ground state stabilized by the JT coupling has an energy lower of a few eV with respect to a different state stabilized by the Hund's coupling. This would place the material in the Mott-bipolaronic region of our phase diagram. A closer connection is hard to establish because of the inherent difficulties to build an effective low-energy model for the low-energy minibands of MATBG [72].

These are some examples that demonstrate that the physics we revealed in our simple model can be realized in real systems of interest. The extension of the present results to three orbitals and/or to different phonon modes is a natural future step of our investigation, as well as the inclusion of material-specific features using a merger of density-functional theory and DMFT.

ACKNOWLEDGMENTS

We acknowledge financial support from Ministero dell'Istruzione, dell'Università e della Ricerca through the PRIN 2017 (Protocol No. 20172H2SC4 005) program and Horizon 2020 through the ERC project FIRSTORM (Grant Agreement No. 692670).

-
- [1] A. J. Millis, P. B. Littlewood, and B. I. Shraiman, *Phys. Rev. Lett.* **74**, 5144 (1995).
- [2] M. Grilli and C. Castellani, *Phys. Rev. B* **50**, 16880 (1994).
- [3] S. Ishihara and N. Nagaosa, *Phys. Rev. B* **69**, 144520 (2004).
- [4] M. L. Kulić, *Phys. Rep.* **338**, 1 (2000).
- [5] O. Gunnarsson and O. Rösch, *J. Phys.: Condens. Matter* **20**, 043201 (2008).
- [6] M. Capone, C. Castellani, and M. Grilli, *Adv. Condens. Matter Phys.* **2010**, 1 (2010).
- [7] Y. Nomura, K. Nakamura, and R. Arita, *Phys. Rev. Lett.* **112**, 027002 (2014).
- [8] S. Choi, S. Johnston, W.-J. Jang, K. Koepernik, K. Nakatsukasa, J. M. Ok, H.-J. Lee, H. W. Choi, A. T. Lee, A. Akbari, Y. K. Semertzidis, Y. Bang, J. S. Kim, and J. Lee, *Phys. Rev. Lett.* **119**, 107003 (2017).
- [9] M. Capone, M. Fabrizio, C. Castellani, and E. Tosatti, *Science* **296**, 2364 (2002).
- [10] J. E. Han, E. Koch, and O. Gunnarsson, *Phys. Rev. Lett.* **84**, 1276 (2000).
- [11] Y. Nomura, S. Sakai, M. Capone, and R. Arita, *Sci. Adv.* **1**, e1500568 (2015).
- [12] Y. Nomura, S. Sakai, M. Capone, and R. Arita, *J. Phys.: Condens. Matter* **28**, 153001 (2016).
- [13] J. K. Freericks and M. Jarrell, *Phys. Rev. Lett.* **75**, 2570 (1995).
- [14] M. Capone, W. Stephan, and M. Grilli, *Phys. Rev. B* **56**, 4484 (1997).
- [15] W. Koller, D. Meyer, and A. C. Hewson, *Phys. Rev. B* **70**, 155103 (2004).
- [16] M. Capone, G. Sangiovanni, C. Castellani, C. Di Castro, and M. Grilli, *Phys. Rev. Lett.* **92**, 106401 (2004).
- [17] G. Sangiovanni, M. Capone, C. Castellani, and M. Grilli, *Phys. Rev. Lett.* **94**, 026401 (2005).
- [18] P. Paci, M. Capone, E. Cappelluti, S. Ciuchi, C. Grimaldi, and L. Pietronero, *Phys. Rev. Lett.* **94**, 036406 (2005).
- [19] C. A. Perroni, V. Cataudella, G. De Filippis, and V. M. Ramaglia, *Phys. Rev. B* **71**, 113107 (2005).
- [20] G. Sangiovanni, M. Capone, and C. Castellani, *Phys. Rev. B* **73**, 165123 (2006).

- [21] P. Barone, R. Raimondi, M. Capone, and C. Castellani, *Phys. Rev. B* **73**, 085120 (2006).
- [22] P. Paci, M. Capone, E. Cappelluti, S. Ciuchi, and C. Grimaldi, *Phys. Rev. B* **74**, 205108 (2006).
- [23] G. Sangiovanni, O. Gunnarsson, E. Koch, C. Castellani, and M. Capone, *Phys. Rev. Lett.* **97**, 046404 (2006).
- [24] A. Macridin, B. Moritz, M. Jarrell, and T. Maier, *Phys. Rev. Lett.* **97**, 056402 (2006).
- [25] M. Tezuka, R. Arita, and H. Aoki, *Phys. Rev. B* **76**, 155114 (2007).
- [26] P. Werner and A. J. Millis, *Phys. Rev. Lett.* **99**, 146404 (2007).
- [27] P. Barone, R. Raimondi, M. Capone, C. Castellani, and M. Fabrizio, *Phys. Rev. B* **77**, 235115 (2008).
- [28] A. Di Ciolo, J. Lorenzana, M. Grilli, and G. Seibold, *Phys. Rev. B* **79**, 085101 (2009).
- [29] J. Bauer and A. C. Hewson, *Phys. Rev. B* **81**, 235113 (2010).
- [30] E. A. Nowadnick, S. Johnston, B. Moritz, R. T. Scalettar, and T. P. Devereaux, *Phys. Rev. Lett.* **109**, 246404 (2012).
- [31] Y. Murakami, P. Werner, N. Tsuji, and H. Aoki, *Phys. Rev. B* **88**, 125126 (2013).
- [32] S. Johnston, E. A. Nowadnick, Y. F. Kung, B. Moritz, R. T. Scalettar, and T. P. Devereaux, *Phys. Rev. B* **87**, 235133 (2013).
- [33] M. Hohenadler and F. F. Assaad, *Phys. Rev. B* **87**, 075149 (2013).
- [34] E. A. Nowadnick, S. Johnston, B. Moritz, and T. P. Devereaux, *Phys. Rev. B* **91**, 165127 (2015).
- [35] T. Ohgoe and M. Imada, *Phys. Rev. Lett.* **119**, 197001 (2017).
- [36] S. Karakuzu, L. F. Tocchio, S. Sorella, and F. Becca, *Phys. Rev. B* **96**, 205145 (2017).
- [37] M. Weber and M. Hohenadler, *Phys. Rev. B* **98**, 085405 (2018).
- [38] A. Ghosh, S. Kar, and S. Yarlagadda, *Eur. Phys. J. B* **91**, 205 (2018).
- [39] N. C. Costa, K. Seki, S. Yunoki, and S. Sorella, *Commun. Phys.* **3**, 80 (2020).
- [40] Y. Wang, I. Esterlis, T. Shi, J. I. Cirac, and E. Demler, *Phys. Rev. Res.* **2**, 043258 (2020).
- [41] Z. Han, S. A. Kivelson, and H. Yao, *Phys. Rev. Lett.* **125**, 167001 (2020).
- [42] C. A. Perroni, E. Piegari, M. Capone, and V. Cataudella, *Phys. Rev. B* **69**, 174301 (2004).
- [43] M. Casula, M. Calandra, and F. Mauri, *Phys. Rev. B* **86**, 075445 (2012).
- [44] G. Giovannetti, M. Casula, P. Werner, F. Mauri, and M. Capone, *Phys. Rev. B* **90**, 115435 (2014).
- [45] E. von Oelsen, A. Di Ciolo, J. Lorenzana, G. Seibold, and M. Grilli, *Phys. Rev. B* **81**, 155116 (2010).
- [46] G. Seibold, M. Grilli, and J. Lorenzana, *Phys. Rev. B* **83**, 174522 (2011).
- [47] J. Sous, M. Chakraborty, C. P. J. Adolphs, R. V. Krems, and M. Berciu, *Sci. Rep.* **7**, 1169 (2017).
- [48] A. Georges, L. de' Medici, and J. Mravlje, *Annu. Rev. Condens. Matter Phys.* **4**, 137 (2013).
- [49] L. de' Medici, J. Mravlje, and A. Georges, *Phys. Rev. Lett.* **107**, 256401 (2011).
- [50] A. Georges, G. Kotliar, W. Krauth, and M. J. Rozenberg, *Rev. Mod. Phys.* **68**, 13 (1996).
- [51] L. de' Medici and M. Capone, in *The Iron Pnictide Superconductors: An Introduction and Overview*, edited by F. Mancini and R. Citro (Springer International Publishing, Cham, 2017), pp. 115–185.
- [52] M. Kim, J. Mravlje, M. Ferrero, O. Parcollet, and A. Georges, *Phys. Rev. Lett.* **120**, 126401 (2018).
- [53] J. E. Han, O. Gunnarsson, and V. H. Crespi, *Phys. Rev. Lett.* **90**, 167006 (2003).
- [54] M. Capone, M. Fabrizio, C. Castellani, and E. Tosatti, *Rev. Mod. Phys.* **81**, 943 (2009).
- [55] Y.-F. Yang and K. Held, *Phys. Rev. B* **76**, 212401 (2007).
- [56] G. Giovannetti, M. Aichhorn, and M. Capone, *Phys. Rev. B* **90**, 245134 (2014).
- [57] A. Carta and C. Ederer, *Phys. Rev. Mater.* **6**, 075004 (2022).
- [58] A. Blason and M. Fabrizio, *Phys. Rev. B* **106**, 235112 (2022).
- [59] C. Castellani, C. R. Natoli, and J. Ranninger, *Phys. Rev. B* **18**, 4945 (1978).
- [60] See Supplemental Material at <http://link.aps.org/supplemental/10.1103/PhysRevB.107.085131> for details about the model, the DMFT parameters, and the behavior of additional observables.
- [61] S. Li, E. Khatami, and S. Johnston, *Phys. Rev. B* **95**, 121112(R) (2017).
- [62] S. Li, Y. Tang, T. A. Maier, and S. Johnston, *Phys. Rev. B* **97**, 195116 (2018).
- [63] J. K. Freericks, M. Jarrell, and D. J. Scalapino, *Phys. Rev. B* **48**, 6302 (1993).
- [64] A. Amaricci, L. Crippa, A. Scazzola, F. Petocchi, G. Mazza, L. de Medici, and M. Capone, *Comput. Phys. Commun.* **273**, 108261 (2022).
- [65] M. Caffarel and W. Krauth, *Phys. Rev. Lett.* **72**, 1545 (1994).
- [66] M. Capone, L. de' Medici, and A. Georges, *Phys. Rev. B* **76**, 245116 (2007).
- [67] M. Capone and S. Ciuchi, *Phys. Rev. Lett.* **91**, 186405 (2003).
- [68] M. Capone, P. Carta, and S. Ciuchi, *Phys. Rev. B* **74**, 045106 (2006).
- [69] A. Isidori, M. Berović, L. Fanfarillo, L. de' Medici, M. Fabrizio, and M. Capone, *Phys. Rev. Lett.* **122**, 186401 (2019).
- [70] A. Richaud, M. Ferraretto, and M. Capone, *Phys. Rev. B* **103**, 205132 (2021).
- [71] L. Crippa, A. Amaricci, S. Adler, G. Sangiovanni, and M. Capone, *Phys. Rev. B* **104**, 235117 (2021).
- [72] L. Zou, H. C. Po, A. Vishwanath, and T. Senthil, *Phys. Rev. B* **98**, 085435 (2018).